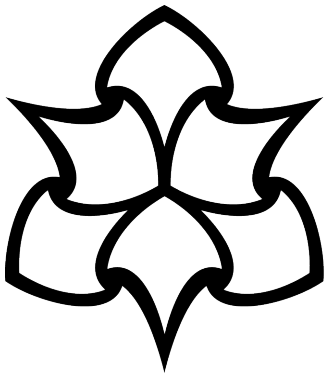

Secure Analysis of Multi-Antenna Cooperative Networks with Residual Transceiver HIs and CEEs

Xingwang Li[1] ✉, *Mengyan Huang*[1], *Jingjing Li*[1], *Qingping Yu*[2], *Khaled Rabie*[3], *Charles C. Cavalcante*[4]

[1] *School of Physics and Electronic Information Engineering, Henan Polytechnic University, Jiaozuo, 45400, China*

[2] *National Key Laboratory of Science and Technology on Communications, University of Electronic Science and Technology of China, Chengdu, China*

[3] *School of Electrical Engineering, Manchester Metropolitan University, Manchester M1 7JW, UK*

[4] *Wireless Telecommunications Research Group, Federal University of Ceará, Campus do Pici, Bl. 722, ZIP 60455-760, Fortaleza-CE, Brazil*

✉ *E-mail: corresponding.lixingwangbupt@gmail.com*

Abstract: In this paper, we investigate the secure performance of multi-antenna decode-and-forward (DF) relaying networks where the Nakagami-m fading channel is taken into account. In practice, the joint impact of residual transceiver hardware impairments (HIs) and channel estimation errors (CEEs) on the outage probability and intercept probability is taken into account. Considering HIs and CEEs, an optimal transmit antenna selection (OTAS) scheme is proposed to enhance the secure performance and then a collaborative eavesdropping scheme is proposed. Additionally, we present main channel capacity and intercept capacity of the multi-antenna DF relaying networks. More specifically, we derive exact closed-form expressions for the outage and intercept probabilities. To obtain useful insights into implications of parameters on the secure performance, the asymptotic behaviors for the outage probability are examined in the high signal-to-noise ratio (SNR) regime and the diversity orders are obtained and discussed. Simulation results confirm the analytical derivations and demonstrate that: 1) As the power distribution coefficient increases, OP decreases, while IP increases; 2) There exist error floors for the outage probability at high SNRs, which is determined by CEEs; 3) The secure performance can be improved by increasing the number of source antennas and artificial noise quantization coefficient, while as the number of eavesdropping increases, the security performance of the system is reduced; 4) There is a trade-off between the outage probability and intercept probability.

1 Introduction

With the development of wireless communication networks (WCNs), the applications of various smart devices have attracted considerable attention, such as internet of things (IoT) [1], device-to-device (D2D) communications [2], machine-to-machine (M2M) communications [3], small cell networks (SCNs) [4] and wearable devices [5]. Owing to the broadcast nature of wireless electromagnetic waves, WCNs become vulnerable to the attack of eavesdroppers, so it is very important to ensure the security of communication systems. Conventional encryption mechanisms can solve this problem by using various encryption algorithms, which impose extra burden for wireless networks [6]. Physical layer security (PLS), which was initially proposed by Wyner [7], has been recognized as a promising technique to provide trustworthy communication. The dominant feature of PLS is to exploit the characteristic of wireless channels to ensure reliable communication links.

Recently, the emerging requirement for secure communication has led to a sizable volume of research on PLS techniques, which focus on the study of the secure performance of WCNs over various fading channels; see e. g., [6, 8–12]. In [8], the authors investigated the secrecy outage performance of multiple-input multiple-output (MIMO) systems over Rayleigh fading channels, where a transmit-beamforming scheme was proposed to maximize the signal-to-noise ratio (SNR) of the main receiver. Considering cooperative cognitive radio networks, a new auxiliary scheme of wireless energy harvesting cooperative jammer (EH-CJ) was proposed to maximize the security rate of the secondary system under the condition of limited transmission power [6]. To characterize the secure performance of line-of-sight (LoS) propagation environments, the authors in [9] analyzed the secrecy capacity of artificial noise aided MIMO systems. In [10], the PLS for the classic Wyner's model over generalized Gamma fading channels was studied by deriving closed-form expressions for secrecy outage probability (SOP) and strictly positive secrecy capacity (SPSC). Regarding the non-homogeneous fading environments, the authors in [11] explored the secrecy performance of Wyner's model over $\alpha-\mu$ fading channels. With the help of moment matching method, the authors in [12] derived approximate expressions for the SOP and SPSC over $\kappa-\mu$ shadowed fading channels.

On a parallel avenue, cooperative relaying is another promising technique to further improve the spectral efficiency and enhance the coverage of wireless networks [13–15], and thus it attracts plenty of researchers to investigate the security issues of cooperative networks [16–23]. In [16], the authors analyzed the secrecy performance of amplify-and-forward (AF) relay systems over generalized-K fading channels, where three metrics for the SOP, average secrecy capacity (ASC) and SPSC were analyzed. To improve the PLS against eavesdropping attacks, the optimal relay selection (ORS) scheme was proposed for AF and decode-and-forward (DF) relay networks and the intercept probability (IP) for the proposed scheme was derived in closed-form [17]. From the perspective of energy harvesting, the authors in [18] proposed a cooperative transmission scheme for the AF and DF relay networks under the condition of an eavesdropper, where the relays can harvest energy from radio-frequency (RF) signals of a source through power-splitting protocol. In the existing research results, the researchers discussed the transmission power under the optimal transmit antenna selection (OTAS) scheme, which can be divided into the following types: 1) The authors of [19] put forward the OTAS scheme for massive MIMO wiretap channels and believed that the transmission power of each antenna is equal and all the power is given to the selected antenna. 2) The authors proposed the OTAS scheme at both the source and relay based on the non-regenerative half-duplex MIMO relay channel, and considered the power to be limited and set the scaling factor to ensure the signal transmits at its expected power constraint [20]. 3) Some researchers

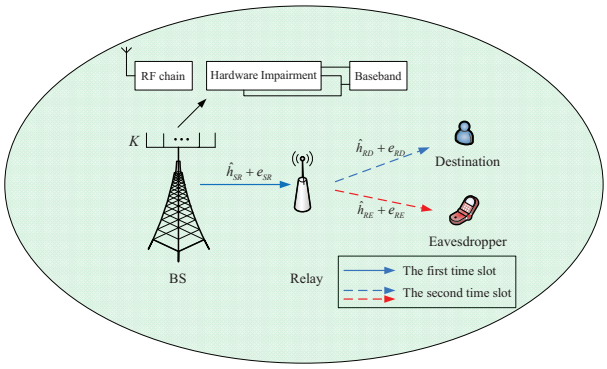

Fig. 1: System model considered HIs and imperfect CSI estimation

studied the transmission power limitation and set the power distribution coefficient to analyze the system performance [21]. Apart from the above works, using stochastic geometry, the work in [22] investigated the PLS of non-orthogonal multiple access (NOMA) in large-scale networks, and the expressions for the SOP of single-antenna and multiple-antenna systems were derived in closed-form. For the cognitive radio based on cooperative systems, the secrecy outage performance was studied over independent but not necessarily identical distributed Nakagami-m fading channels by Lei et al. [23, 24], and three representative relay selection schemes were proposed, namely, ORS, suboptimal relay selection (SRS) and multiple relays combining (MRC).

Antenna selection technology in MIMO systems is similar to relay selection. In the case that multiple antennas are available at the source node and the optimal antenna is selected from all antennas for use under certain condition, the advantages of spatial diversity or multiplexing of cooperative relay communication networks can be brought into play and the implementation complexity of the relay process can be reduced. In an actual communication system, due to the broadcast characteristics of wireless communication, the wireless network lacks a secure physical boundary, and wireless communication without physical connection is open to external eavesdroppers. There are two ways for eavesdroppers to intercept information: 1) non-collaborative eavesdroppers [25]; 2) collaborative eavesdroppers [26]. However, because the synchronization and the internal information exchange are not perfected, it is difficult for multiple eavesdroppers to intercept the legally transmitted information at the same time, thereby reducing the confidentiality of the cooperative communication.

Clearly, the aforementioned research works are limited to the assumption of hardware impairments (HIs). In practice, the transceivers of wireless systems suffer from some types of hardware imperfections, such as in-phase/quadrature-phase (I/Q) imbalance, phase noise, high-power amplifier non-linearity etc. [27–30]. Although these impairments can usually be mitigated with the help of some compensation algorithms, due to the inherent characteristics of RF components, the HIs cannot be fully removed. There are some residual hardware impairments (RHIs) because of imperfect estimation and time variation [29]. It has been proved that the RHIs can be modeled as additive noise with certain characteristics [31]. In addition, inaccurate channel state information (CSI) is very likely to be present due to the existence of channel estimation errors (CEEs) [32–36]. Therefore, it is of high practical relevance to consider the imperfect CSI for secure performance of cooperative relay networks.

Previous research works have provided a foundation for knowledge of cooperative communication and PLS. Motivated by these observations, we focus on the secure performance of multi-antenna DF relay networks in terms of outage probability (OP) and IP, where two practical deleterious factors are considered: i) RHIs; ii) CEEs. Also, the general Nakagami-m fading channel has been considered since it is widely used to represent fading characteristics of various wireless propagation environments. By setting different parameters, Nakagami-m fading channels can be reduced to Rayleigh (m = 1) and Gaussian (m = 1/2). Moreover, the OTAS scheme is proposed to maximize the SNR of the link between the source and relay. To characterize the secure performance of the considered networks, the exact closed-form expressions for the OP and IP of DF relaying networks in the presence of HIs and CEEs are derived. To obtain useful insights, the asymptotic behaviors in the high SNR regime and the diversity orders of OP are explored. The primary contributions of this paper can be summarized as follows:

• We propose an OTAS scheme to maximize the SNR of the link between the source and relay. Contrary to most existing works, the effect of HIs and CEEs is taken into account in this current study. In addition, two representative CEE assumptions are considered: 1) The estimated error is a fixed constant; 2) The estimated error is a function of transmitted average SNR.

• Based on the proposed OTAS scheme and collaborative eavesdropping strategy, we investigate the reliability and security performance of multi-antenna DF relay networks over Nakagami-m fading channels. To characterize the performance, we derive the exact closed-form expressions for the OP and IP of the considered communication system. The results reveal that deploying more antennas at the transmitter enhances the reliability whereas increasing the number of antennas at interceptor degrades the security; on the other hand, while increasing artificial noise quantization coefficient reduces IP.

• To obtain more insights, the asymptotic performance for the OP is explored with the consideration of eavesdropping. It is demonstrated that the reliability suffers from HIs and CEEs, while HIs and CEEs are always beneficial for reducing IP. This means that HIs and CEEs are useful to enhance security. Besides, there is error floor for the OP under high SNR region in the presence of fixed CEEs, which is irrelative to the transmitted power. It is also shown that there is a trade-off between OP and IP.

The rest of this paper is introduced as follows. In Section 2, we present the system model of the considered networks. In Section 3, after presenting the source antenna selection and collaborative eavesdropper schemes, we investigate the security and reliability by deriving the OP and IP of the considered networks. In Section 4, the asymptotic behavior and diversity orders for the OP at high SNRs are analyzed and discussed. Numerical results are presented to verify the derived results in Section 5, and the impacts of number of antennas, HIs and CEEs on the system performance can be obtained through the provided numerical results. Finally, Section 6 summarized this paper.

Notations: In this paper, the $\mathcal{CN}\left(u, \sigma^2\right)$ denotes the complex Gaussian random variable with mean u and variance σ^2. The $\mathrm{E}\{\cdot\}$ and $\Pr(\cdot)$ denote the expected operator and probability, respectively. Notation $\mathcal{G}(\alpha, \beta)$ means the Gamma distribution. $f_X(\cdot)$ and $F_X(\cdot)$ are the probability density function (PDF) and the cumulative distribution function (CDF) of a random variable, respectively. The $\log(\cdot)$ is the logarithm. Finally, the $|\cdot|$ and $(\cdot)!$ denote absolute value and factorial, respectively.

2 System Model and Statistical Characteristics

In this section, we present the system model and the statistical characteristics of the fading channels used in the secure performance analysis in Sections 3 and 4.

2.1 System Model

We consider a system model illustrated in Fig. 1. There is one transmitter S (e.g., a base station), one relay R, one legitimate destination D and one illegitimate eavesdropper E. We assume that R and D are equipped with one antenna, while S has K antennas $\{S_1, S_2, \cdots, S_k, \cdots, S_K\}$ and E has N antennas $\{E_1, E_2, \cdots, E_n, \cdots, E_N\}$. In this study, DF protocol is considered. We also assume that there are no direct links between the following nodes $S_k \to D$ and $S_k \to E_n$ due to shadow fading, which is a widely used assumption in the literature [17, 18].

The communication process is divided into two time slots: 1) S transmits its own signal to R; 2) R decodes and forwards the

received signals to D. To enhance the secure performance, the artificial noise signal is sent to D and E_n. In practice, it is a great challenge to obtain CSI at all nodes, and hence channel estimation is often implemented [32–36]. The most common approach is to estimate the channel by using training sequence. Utilizing linear minimum mean-square error (LMMSE), the real channel can be written as [34]:

$$h_{XY} = \hat{h}_{XY} + e_{XY}, \tag{1}$$

where $XY \in \{S_kR; RD; RE_n\}, (1 \le k \le K, 1 \le n \le N)$, $\hat{h}_{XY}$ is the estimated channel of h_{XY}, $e_{XY} \sim \mathcal{CN}\left(0, \sigma^2_{e_{XY}}\right)$ is the CEE, where $\sigma^2_{e_{XY}}$ is the variance of estimation. In this study, we consider two representative channel estimation models: 1) The variance of CEE is a non-negative fixed constant; 2) The variance of CEE is a function of transmit average SNR, which can be modeled as $\sigma^2_{e_{XY}} = \Omega_{XY}/(1 + \delta\rho_{XY}\Omega_{XY})$, where Ω_{XY} and ρ_{XY} are the variance of channel gain and transmit average SNR, respectively; $\delta > 0$ is the channel estimation quality parameter, which represents the power consumption of training pilots to acquiring CSI [33].

1) The first time slot: In this phase, the signal x_{S_kR} is transmitted to R, where $\mathrm{E}\left\{|x_{S_kR}|^2\right\} = 1$. We considering RHIs and imperfect CSI, the received signal at the R is expressed as:

$$y_{S_kR} = \left(\hat{h}_{S_kR} + e_{S_kR}\right)\left(\sqrt{P_S}x_{S_kR} + \eta_{t,S_kR}\right) + \eta_{r,S_kR} + v_{S_kR}, \tag{2}$$

where $\hat{h}_{S_kR}$ is the fading channel between the selected transmit antenna and R, and the OTSA criterion is provided in the next section; x_{S_kR} is the effective signal of $S_k \to R$ and $\mathrm{E}|x_{S_kR}|^2 = 1$; $v_{S_kR} \sim \mathcal{CN}\left(0, \sigma^2_{S_kR}\right)$ is the complex additive white Gaussian noise (AWGN); P_S is the transmit power from S. Note that in practice, the transmitting power of the system is limited, $P_S = \mu P$, P is the total power in the source, μ is the power allocation factor on the selected antenna and $1 - \mu$ is the power allocation factor on the other antennas; η_{t,S_kR} and η_{r,S_kR} are the distortion noises from HIs at the transmitter and receiver, respectively.

2) The second time slot: At R, the received signal is decoded and forwarded to D and E_n. To improve the secure performance, the R transmits artificial noise signal to D and E_n at the same time. In practice, D can not remove the artificial noise due to the CEEs, and there are some residual interference received at D [37–39]. Therefore, the received signals at D and E_n can be expressed as:

$$y_{RD} = \left(\hat{h}_{RD} + e_{RD}\right)\left(\sqrt{P_R}x_{RD} + \sqrt{\xi_1 P_J}x_{J_{RD}} + \eta_{t,RD}\right) + \eta_{r,RD} + v_{RD}, \tag{3}$$

$$y_{RE_n} = \left(\hat{h}_{RE_n} + e_{RE_n}\right)\left(\sqrt{P_R}x_{RE_n} + \sqrt{\xi_2 P_J}x_{J_{RE_n}} + \eta_{t,RE_n}\right) + \eta_{r,RE_n} + v_{RE_n}, \tag{4}$$

where x_{RD} and x_{RE_n} are the signal sending to D and E_n with $E|x_{RD}|^2 = E|x_{RE_n}|^2 = 1$, respectively; $x_{J_{RD}}$, $x_{J_{RE_n}}$ are the signal sending to D and E_n with $E|x_{J_{RD}}|^2 = E|x_{J_{RE_n}}|^2 = 1$, respectively; $\xi_1 \in (0,1)$ and $\xi_2 \in (0,1)$ are the quantization coefficients of the artificial noise on D and E_n, respectively; $v_{RD} \sim \mathcal{CN}\left(0, \sigma^2_{RD}\right)$ and $v_{RE_n} \sim \mathcal{CN}\left(0, \sigma^2_{RE_n}\right)$ are the complex AWGN; P_R is the average transmit power at R, P_J is the power used to transmit the artificial noise and $P_R = P_S = P_g$; $\eta_{t,RD}$, $\eta_{r,RD}$ are distortion noises of the transmitter and receiver for $R \to D$ transmission channel, respectively; η_{t,RE_n}, η_{r,RE_n} are distortion noises of the transmitter and receiver for $R \to E_n$ transmission channel, respectively. As stated in [40], the distortion noises are defined as

$$\eta_{t,XY} \sim CN\left(0, \kappa^2_{t,XY}P_g\right), \eta_{r,XY} \sim CN\left(0, \kappa^2_{r,XY}P_g|h_{XY}|^2\right), \tag{5}$$

the effective distortion noise can be seen as two independent jointly Gaussian variable $\eta_{t,XY}$ and $\eta_{r,XY}/h_{XY}$ that are multiplied with the fading channel h_{XY}. For a given channel realization h_{XY}, the aggregated distortion seen at the receiver has power

$$\begin{aligned}\mathrm{E}_{\eta_{t,XY},\eta_{r,XY}}\left\{\left|h_{XY}\eta_{t,XY} + \eta_{r,XY}\right|^2\right\} &= P_g|h_{XY}|^2\left(\kappa^2_{t,XY} + \kappa^2_{r,XY}\right) \\ &= P_g\left|\hat{h}_{XY} + e_{XY}\right|^2\left(\kappa^2_{t,XY} + \kappa^2_{r,XY}\right),\end{aligned} \tag{6}$$

we can observe that it only depends on the average signal power P_g and the instantaneous channel gain $|h_{XY}|^2$. We have the definition that $\kappa_{XY} = \sqrt{\kappa^2_{t,XY} + \kappa^2_{r,XY}}$. Thus, the received signals at R, D and E_n can be respectively rewritten as:

$$y_{S_kR} = \left(\hat{h}_{S_kR} + e_{S_kR}\right)\left(\sqrt{P_S}x_{S_kR} + \eta_{S_kR}\right) + v_{S_kR}, \tag{7}$$

$$y_{RD} = \left(\hat{h}_{RD} + e_{RD}\right)\left(\sqrt{P_R}x_{RD} + \sqrt{\xi_1 P_J}x_{J_{RD}} + \eta_{RD}\right) + v_{RD}, \tag{8}$$

$$y_{RE_n} = \left(\hat{h}_{RE_n} + e_{RE_n}\right)\left(\sqrt{P_R}x_{RE_n} + \sqrt{\xi_2 P_J}x_{J_{RE_n}} + \eta_{RE_n}\right) + v_{RE_n}, \tag{9}$$

where $\eta_{S_kR} \sim \mathcal{CN}\left(0, \kappa^2_{S_kR}P_S\right)$, $\eta_{RD} \sim \mathcal{CN}\left(0, \kappa^2_{RD}P_R\right)$ and $\eta_{RE_n} \sim \mathcal{CN}\left(0, \kappa^2_{RE_n}P_R\right)$ are the aggregated distortion noises from RHIs at $S_k \to R$, $R \to D$ and $R \to E_n$, respectively; such that, $\kappa_{S_kR} \triangleq \sqrt{\kappa^2_{t,S_kR} + \kappa^2_{r,S_kR}}$, $\kappa_{RD} \triangleq \sqrt{\kappa^2_{t,RD} + \kappa^2_{r,RD}}$ and $\kappa_{RE_n} \triangleq \sqrt{\kappa^2_{t,RE_n} + \kappa^2_{r,RE_n}}$.

According to (7), (8) and (9), the effective signal-to-interference plus noise ratios (SINRs) of the links $S_k \to R$, $R \to D$ and $R \to E_n$ are given as [34]:

$$\gamma_{S_kR} = \frac{\rho_{S_kR}\left|\hat{h}_{S_kR}\right|^2}{\rho_{S_kR}\left(\sigma^2_{e_{S_kR}} + \left|\hat{h}_{S_kR}\right|^2\kappa^2_{S_kR} + \sigma^2_{e_{S_kR}}\kappa^2_{S_kR}\right) + 1}, \tag{10}$$

$$\gamma_{RD} = \frac{\rho_{RD}\left|\hat{h}_{RD}\right|^2}{\sigma^2_{e_{RD}}\rho_{RD} + \left(\xi_1 P_J\Big/\sigma^2_{RD} + \kappa^2_{RD}\rho_{RD}\right)\left(\left|\hat{h}_{RD}\right|^2 + \sigma^2_{e_{RD}}\right) + 1}, \tag{11}$$

$$\gamma_{RE_n} = \frac{\rho_{RE_n}\left|\hat{h}_{RE_n}\right|^2}{\sigma^2_{e_{RE_n}}\rho_{RE_n} + \left(\xi_2 P_J\Big/\sigma^2_{RE_n} + \kappa^2_{RE_n}\rho_{RE_n}\right)\left(\left|\hat{h}_{RE_n}\right|^2 + \sigma^2_{e_{RE_n}}\right) + 1}, \tag{12}$$

where $\rho_{S_kR} = P_S\Big/\sigma^2_{S_kR}$, $\rho_{RD} = P_R\Big/\sigma^2_{RD}$ and $\rho_{RE_n} = P_R\Big/\sigma^2_{RE_n}$.

2.2 Statistical Characteristics

In this study, the generic Nakagami-m fading channel is adopted, in which the channel amplitudes $\left|\hat{h}_{XY}\right|$ follows independent but non-identically Nakagami-m distribution. Then the channel gain follows Gamma distribution with $\left|\hat{h}_{XY}\right|^2 \sim \mathcal{G}\left(\alpha_{XY}, \beta_{XY}\right)$, where $\alpha_{XY} \ge 1$ and $\beta_{XY} > 0$ are the shape parameters and scale parameter, respectively. Thus, the PDF and the CDF of the channel gains can be expressed as [40]:

$$f_{|\hat{h}_{XY}|^2}(x) = \frac{x^{\alpha_{XY}-1}e^{-\frac{x}{\beta_{XY}}}}{\Gamma\left(\alpha_{XY}\right)\beta^{\alpha_{XY}}_{XY}}, x \ge 0, \tag{13}$$

$$F_{|\hat{h}_{XY}|^2}(x) = 1 - \sum_{l=0}^{\alpha_{XY}-1}\frac{e^{-\frac{x}{\beta_{XY}}}}{l!}\left(\frac{x}{\beta_{XY}}\right)^l, x \ge 0. \tag{14}$$

According to Shannon's capacity formula, we can obtain the instantaneous channel capacity as [39]:

$$C_{XY} = \frac{1}{2}\log_2\left(1+\gamma_{XY}\right), \tag{15}$$

where γ_{XY} denotes the SINR from transmitter to receiver.

3 Performance Analyses of the Outage Probability and Intercept Probability

In this section, we first propose an OTAS strategy to enhance the security performance, then the reliability and security are investigated by deriving the exact closed-form expressions for the OP and IP.

3.1 OP Analysis

In the following, we investigate the reliability considered multi-antenna cooperative networks in the presence of RHIs and CEEs in terms of OP.

Outage Probability: For a target transmission rate R_S, the probability of outage event $C_{S_kR} < R_S$ or outage event $C_{RD} < R_S$ occurring on the two transmission processes of $S_k \to R$ and $R \to D$. With this in mind, the OP can be expressed as:

$$P_{\text{out}} = \Pr\left\{C_R < R_S\right\}. \tag{16}$$

The specific calculation and the meaning of the symbol are described below.

Optimal Transmit Antenna Selection: In this subsection, an OTAS strategy is proposed. Contrary to the existing works, RHIs at transceivers and CEEs are taken into account. For OTAS, one of the transmit antennas is selected according to the largest channel gain between the antennas. Thus, the corresponding mathematical formal can be expressed as:

$$\hat{h}_{SR} = \max_{1\le k\le K}\left\{\hat{h}_{S_kR}\right\}. \tag{17}$$

Therefore, the PDF and CDF of the channel gain in the first time slot can be expressed as:

$$f_{\left|\hat{h}_{SR}\right|^2}(x) = \frac{Ke^{-\frac{x}{\beta_{SR}}}}{\beta_{SR}^{\alpha_{SR}}(\alpha_{SR}-1)!}x^{\alpha_{SR}-1}\left[1-\sum_{j=0}^{\alpha_{SR}-1}\frac{e^{-\frac{x}{\beta_{SR}}}}{j!}\left(\frac{x}{\beta_{SR}}\right)^j\right]^{K-1}, x\ge 0, \tag{18}$$

$$F_{\left|\hat{h}_{SR}\right|^2}(x) = \left[1-\sum_{j=0}^{\alpha_{SR}-1}\frac{e^{-\frac{x}{\beta_{SR}}}}{j!}\left(\frac{x}{\beta_{SR}}\right)^j\right]^K, x\ge 0. \tag{19}$$

Based on (15), the instantaneous channel capacities of $S \to R$ and $R \to D$ can be further re-expressed as:

$$C_{SR} = \frac{1}{2}\log_2\left(1+\frac{\rho_{SR}\left|\hat{h}_{SR}\right|^2}{\rho_{SR}\left(\sigma_{e_{SR}}^2+\left|\hat{h}_{SR}\right|^2\kappa_{SR}^2+\sigma_{e_{SR}}^2\kappa_{SR}^2\right)+1}\right), \tag{20}$$

$$C_{RD} = \frac{1}{2}\log_2\left(1+\frac{\rho_{RD}\left|\hat{h}_{RD}\right|^2}{\sigma_{e_{RD}}^2\rho_{RD}+\left(\xi_1P_J\Big/\sigma_{RD}^2+\kappa_{RD}^2\rho_{RD}\right)\left(\left|\hat{h}_{RD}\right|^2+\sigma_{e_{RD}}^2\right)+1}\right), \tag{21}$$

where $\rho_{SR} = P_s\Big/\sigma_{SR}^2$.

According to the criterion of DF protocol, the end-to-end channel capacity is the minimum of channel capacities $S \to R$ and $R \to D$. Thus,

$$C_R = \min\left(C_{SR}, C_{RD}\right). \tag{22}$$

Utilizing the above definition, the exact closed-form expressions for the OP are provided over Nakagami-m fading channels with RHIs and CEEs in the following theorem.

Theorem 1. *For Nakagami-m fading channels, the exact analytical expressions for the OP are given as*

• *Non-ideal condition (with HIs and CEEs)*

$$P_{\text{out}}^{\text{ni}} = \left[1-\sum_{j=0}^{\alpha_{SR}-1}\frac{e^{-\frac{\Theta_1}{\beta_{SR}}}}{j!}\left(\frac{\Theta_1}{\beta_{SR}}\right)^j\right]^K + 1 - \sum_{l=0}^{\alpha_{RD}-1}\frac{e^{-\frac{\Theta_2}{\beta_{RD}}}}{l!}\left(\frac{\Theta_2}{\beta_{RD}}\right)^l - \left[1-\sum_{j=0}^{\alpha_{SR}-1}\frac{e^{-\frac{\Theta_1}{\beta_{SR}}}}{j!}\left(\frac{\Theta_1}{\beta_{SR}}\right)^j\right]^K\left[1-\sum_{l=0}^{\alpha_{RD}-1}\frac{e^{-\frac{\Theta_2}{\beta_{RD}}}}{l!}\left(\frac{\Theta_2}{\beta_{RD}}\right)^l\right], \tag{23}$$

where $\varepsilon = 2^{2R_S}-1$, $\Theta_1 = \frac{\varepsilon\rho_{SR}\sigma_{e_{SR}}^2\left(1+\kappa_{SR}^2\right)+\varepsilon}{\rho_{SR}\left(1-\varepsilon\kappa_{SR}^2\right)}$ and $\Theta_2 = \frac{\varepsilon\left[\sigma_{e_{RD}}^2\left(\rho_{RD}+\xi_1P_J/\sigma_{RD}^2+\kappa_{RD}^2\rho_{RD}\right)+1\right]}{\rho_{RD}-\varepsilon\left(\xi_1P_J/\sigma_{RD}^2+\kappa_{RD}^2\rho_{RD}\right)}$. In this case, we assume that $1-\varepsilon\kappa_{SR}^2 > 0$ and $\rho_{RD}-\varepsilon\left(\xi_1P_J\Big/\sigma_{RD}^2+\kappa_{RD}^2\rho_{RD}\right) > 0$, otherwise the OP is zero.

• *Ideal condition ($\kappa_{SR} = \kappa_{RD} = 0$ and $\sigma_{e_{SR}}^2 = \sigma_{e_{RD}}^2 = 0$)*

$$P_{\text{out}}^{\text{id}} = \left[1-\sum_{j=0}^{\alpha_{SR}-1}\frac{e^{-\frac{\Theta_3}{\beta_{SR}}}}{j!}\left(\frac{\Theta_3}{\beta_{SR}}\right)^j\right]^K + 1 - \sum_{l=0}^{\alpha_{RD}-1}\frac{e^{-\frac{\Theta_4}{\beta_{RD}}}}{l!}\left(\frac{\Theta_4}{\beta_{RD}}\right)^l - \left[1-\sum_{j=0}^{\alpha_{SR}-1}\frac{e^{-\frac{\Theta_3}{\beta_{SR}}}}{j!}\left(\frac{\Theta_3}{\beta_{SR}}\right)^j\right]^K\left[1-\sum_{l=0}^{\alpha_{RD}-1}\frac{e^{-\frac{\Theta_4}{\beta_{RD}}}}{l!}\left(\frac{\Theta_4}{\beta_{RD}}\right)^l\right], \tag{24}$$

where $\Theta_3 = \frac{\varepsilon}{\rho_{SR}}$, $\Theta_4 = \frac{\varepsilon}{\rho_{RD}-\varepsilon\xi_1P_J/\sigma_{RD}^2}$.

Proof: See Appendix A. □

3.2 IP Analysis

In this subsection, we analyze the secrecy performance of the considered multi-antenna and multi-eavesdropper cooperative networks in the presence of RHIs and CEEs in terms of IP, which is defined as the probability that the capacity of the main link ($S_k \to R \to D_n$) is less than that of the wiretap link.

Intercept Probability: In this case, the eavesdropper most likely succeeds to intercept the legitimate information. In mathematics, IP corresponds to the probability of zero secrecy rate event, which is expressed as [26]:

$$P_{\text{int}} = \Pr\left\{C_{RE} > R_S\right\}, \tag{25}$$

the specific meaning of the symbol is as follows.

Collaborative Eavesdropper Scheme: Here, collaborative eavesdropping scheme is considered to eavesdrop the legitimate information. Using the MRC method, the SINR of $R \to E$ is:

$$\gamma_{RE} = \sum_{n=1}^{N}\gamma_{RE_n}. \tag{26}$$

1) Non-independent identical distribution: substituting (26) into (25), the following expression can be obtained as:

$$P_{\text{int}}^{\text{n.i.i.d}} = \Pr\left\{\sum_{n=1}^{N}\frac{\rho_{RE_n}\left|\hat{h}_{RE_n}\right|^2}{\sigma_{e_{RE_n}}^2\rho_{RE_n}+\left(\frac{\xi_2P_J}{\sigma_{RE_n}^2}+\kappa_{RE_n}^2\rho_{RE_n}\right)\left(\left|\hat{h}_{RE_n}\right|^2+\sigma_{e_{RE_n}}^2\right)+1} > \varepsilon\right\}, \tag{27}$$

obviously, it is difficult, if not impossible, to derive the expression for the IP. To circumvent this problem, the asymptotic IP in the low

SNR regime is investigated. According to (27), the asymptotic IP can be written as:

$$P_{\text{int,asy}}^{\text{n.i.i.d}} = 1 - \frac{1}{\Gamma(N\alpha_{RE_n})\,\beta_{RE_n}^{N\alpha_{RE_n}}} \Upsilon\left(N\alpha_{RE_n}, \frac{\varepsilon}{\beta_{RE_n}\rho_{RE_n}}\right). \quad (28)$$

2) Independent identical distribution: because it is difficult to figure out the non-independent identical distribution in the MRC case, we consider each SINR of $R \to E_n$ to be independently and identically distributed under the collaborative eavesdropper scheme. Note that in fact, SINRs for all eavesdroppers are different since different eavesdroppers are, in general geographically separated. To maintain mathematical tractability and obtain engineering insight, we have adopted this simplified. Hence, the following can be obtained [41]:

$$\gamma_{RE} = N\gamma_{RE_n}. \quad (29)$$

According to (15), we can obtain the eavesdropping capacity from $R \to E$ under the collaborative eavesdropping scheme as follows:

$$C_{RE} = \frac{1}{2}\log_2\left(1 + N\gamma_{RE_n}\right). \quad (30)$$

Similarly, the following theorem explores the security performance in term of IP over Nakagami-m fading channels with HIs and CEEs.

Theorem 2. *For Nakagami-m fading channels, the exact analytical expressions for the IP are given as*

• *Non-ideal condition*

$$P_{\text{int,i.i.d}}^{\text{ni}} = \sum_{l=0}^{\alpha_{RE_n}-1} \frac{e^{-\frac{\Theta_5}{\beta_{RE_n}}}}{l!}\left(\frac{\Theta_5}{\beta_{RE_n}}\right)^l, \quad (31)$$

where $\Theta_5 = \frac{\varphi\left[\sigma_{e_{RE_n}}^2\left(\rho_{RE_n}+\xi_2 P_J/\sigma_{RE_n}^2+\kappa_{RE_n}^2\rho_{RE_n}\right)+1\right]}{\rho_{RE_n}-\varphi\left(\xi_2 P_J/\sigma_{RE_n}^2+\kappa_{RE_n}^2\rho_{RE_n}\right)}$, $\varepsilon = 2^{2R_S}-1$, $\varphi = \frac{\varepsilon}{N}$ and in there, we should be ensure that $\varphi < \frac{\rho_{RE_n}}{\xi_2 P_J/\sigma_{RE_n}^2+\kappa_{RE_n}^2\rho_{RE_n}}$, otherwise the IP is one.

• *Ideal condition*

$$P_{\text{int}}^{\text{id}} = \sum_{l=0}^{\alpha_{RE}-1} \frac{e^{-\frac{\Theta_6}{\beta_{RE}}}}{l!}\left(\frac{\Theta_6}{\beta_{RE}}\right)^l, \quad (32)$$

where $\Theta_6 = \frac{\varphi}{\rho_{RE_n}-\varphi\xi_2 P_J/\sigma_{RE_n}^2}$, $\varepsilon = 2^{2R_S}-1$, $\varphi = \frac{\varepsilon}{N}$ and ensure the $\varphi < \frac{\rho_{RE_n}\sigma_{RE_n}^2}{\xi_2 P_J}$.

Proof: See Appendix B. □

From **Theorem 1** and **Theorem 2**, we can observe that the OP and IP are determined by the number of transmit antennas, fading parameters, RHIs and CEEs. Although the above results can be expressed in closed-form, they do not provide useful insights into the implication of system parameters on the reliability and security performance. To this end, the asymptotic behaviors for the OP are examined in the following section.

4 Asymptotic Analysis

To reveal useful insights, the following corollaries provide the asymptotic analysis and the diversity order for the OP in the high SNR region.

4.1 High SNRs Analysis

Corollary 1. *At high SNRs ($\rho_{XY} \to \infty$), the asymptotic expressions of OP for the cooperative communication system are given by*

• *Non-ideal condition*

1) When the $\sigma_{e_{XY}}^2 = \frac{\Omega_{XY}}{1+\delta\rho_{XY}\Omega_{XY}}$:

$$\begin{aligned} P_{\text{out}}^{\infty,\text{ni1}} &= I_3 + I_4 - I_3 I_4 \\ &= \left(\frac{\Theta_1^{\alpha_{SR}}}{\alpha_{SR}!\beta_{SR}^{\alpha_{SR}}}\right)^K + \frac{\Theta_2^{\alpha_{RD}}}{\alpha_{RD}!\beta_{RD}^{\alpha_{RD}}} - \left(\frac{\Theta_1^{\alpha_{SR}}}{\alpha_{SR}!\beta_{SR}^{\alpha_{SR}}}\right)^K \left(\frac{\Theta_2^{\alpha_{RD}}}{\alpha_{RD}!\beta_{RD}^{\alpha_{RD}}}\right) \end{aligned}. \quad (33)$$

2) When the $\sigma_{e_{XY}}^2 = a$ (a is a constant):

$$\begin{aligned} P_{\text{out}}^{\infty,\text{ni2}} = &\left[1 - \sum_{j=0}^{\alpha_{SR}-1} \frac{e^{-\frac{\Theta_7}{\beta_{SR}}}}{j!}\left(\frac{\Theta_7}{\beta_{SR}}\right)^j\right]^K + \left[1 - \sum_{l=0}^{\alpha_{RD}-1} \frac{e^{-\frac{\Theta_8}{\beta_{RD}}}}{l!}\left(\frac{\Theta_8}{\beta_{RD}}\right)^l\right] \\ &- \left[1 - \sum_{j=0}^{\alpha_{SR}-1} \frac{e^{-\frac{\Theta_7}{\beta_{SR}}}}{j!}\left(\frac{\Theta_7}{\beta_{SR}}\right)^j\right]^K \left[1 - \sum_{l=0}^{\alpha_{RD}-1} \frac{e^{-\frac{\Theta_8}{\beta_{RD}}}}{l!}\left(\frac{\Theta_8}{\beta_{RD}}\right)^l\right] \end{aligned}, \quad (34)$$

where $\Theta_7 = \frac{\varepsilon\sigma_{e_{SR}}^2\left(1+\kappa_{SR}^2\right)}{1-\varepsilon\kappa_{SR}^2}$, $\Theta_8 = \frac{\varepsilon\sigma_{e_{RD}}^2\left(1+\xi_1/2+\kappa_{RD}^2\right)}{1-\varepsilon\xi_1/2-\varepsilon\kappa_{RD}^2}$ and we should ensure $1-\varepsilon\kappa_{SR}^2 > 0$ and $1-\varepsilon\xi_1/2-\varepsilon\kappa_{RD}^2 > 0$.

• *Ideal condition*

$$\begin{aligned} P_{\text{out}}^{\infty,\text{id}} = &\left(\frac{\Theta_3^{\alpha_{SR}}}{\alpha_{SR}!\beta_{SR}^{\alpha_{SR}}}\right)^K + \frac{\Theta_4^{\alpha_{RD}}}{\alpha_{RD}!\beta_{RD}^{\alpha_{RD}}} \\ &- \left(\frac{\Theta_3^{\alpha_{SR}}}{\alpha_{SR}!\beta_{SR}^{\alpha_{SR}}}\right)^K \left[\frac{\Theta_4^{\alpha_{RD}}}{\alpha_{RD}!\beta_{RD}^{\alpha_{RD}}}\right] \end{aligned}. \quad (35)$$

Proof: See Appendix C. □

Remark 1. *From **Corollary 1**, we can obtain the following observations as: 1) For non-ideal conditions, when the $\sigma_{e_{XY}}^2 = \frac{\Omega_{XY}}{1+\delta\rho_{XY}\Omega_{XY}}$, the asymptotic outage performance changes with the changes of the average transmit SNR; when the $\sigma_{e_{XY}}^2 = a$, the OP is a fixed constant when the transmit SNR grows very large, which means that the outage performance cannot always be improved by increasing the transmit power; 2) For ideal conditions, the asymptotic OP also varies with the change of average transmit SNR.*

4.2 Diversity Order

To obtain more insights, the diversity order is explored, which is defined as [42]

$$d = -\lim_{\rho\to\infty} \frac{\log\left(P_{\text{out}}^{\infty}\right)}{\log\rho}, \quad (36)$$

where ρ is average transmit SNR and P_{out}^{∞} is asymptotic analytical expression of OP.

Corollary 2. *The diversity orders under non-ideal and ideal conditions are given by*

• *Non-ideal condition*

1) When the $\sigma_{e_{XY}}^2 = \frac{\Omega_{XY}}{1+\delta\rho_{XY}\Omega_{XY}}$:

$$d^{\text{ni1}}\left(\rho_{SR}, \rho_{RD}\right) = \min\left(K\alpha_{SR}, \alpha_{RD}\right). \quad (37)$$

2)When the $\sigma_{e_{XY}}^2 = a$:

$$d^{\text{ni2}}\left(\rho_{SR}, \rho_{RD}\right) = 0. \quad (38)$$

Proof: Based on the results of (33) and (34), we can have the following proof in the non-ideal case. For the channel estimation error

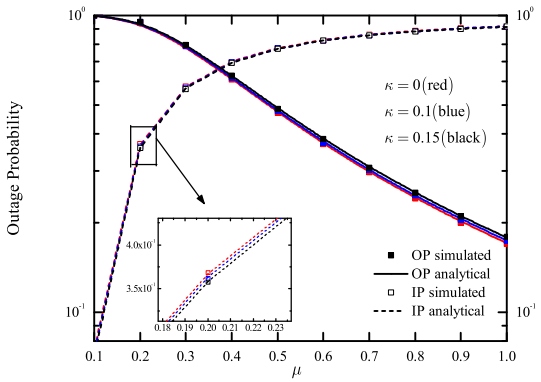

Fig. 2: OP and IP versus μ for different κ ($\alpha = 2$, $\{\xi_1, \xi_2\} = \{0.02, 0.99\}$, $SNR = 5dB$, $\sigma_e^2 = 0.05$, $N = 2$ and $K = 2$)

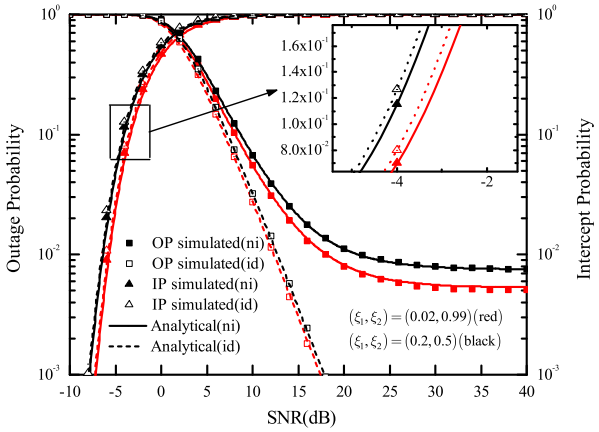

Fig. 3: OP and IP versus SNR for different $\{\xi_1, \xi_2\}$ ($\alpha = 2, \mu = 0.8, \sigma_e^2 = 0.1, \kappa = 0.15, N = 2$ and $K = 2$)

parameters are variables, the dominant terms of (33) are:

$$P_{\text{out}}^{\infty,\text{ni1}} = \left(\frac{{\Theta_1}^{\alpha_{SR}}}{\alpha_{SR}! \beta_{SR}^{\alpha_{SR}}} \right)^K + \frac{{\Theta_2}^{\alpha_{RD}}}{\alpha_{RD}! \beta_{RD}^{\alpha_{RD}}}. \tag{39}$$

Substituting (39) into (36), after some manipulations, we can obtain (37).

Then, substitute (34) into (36). Since (34) is a constant, the diversity order is zero, and then (38) can be obtained. □

• *Ideal condition*

$$d^{\text{id}}(\rho_{SR}, \rho_{RD}) = \min(K\alpha_{SR}, \alpha_{RD}). \tag{40}$$

Proof: Based on the results of (33), we have the proof of ideal conditions. Substituting (33) into (34) yields the result of (38).

For ideal conditions, the dominant terms of (35) are:

$$P_{\text{out}}^{\infty,\text{id}} = \left(\frac{{\Theta_3}^{\alpha_{SR}}}{\alpha_{SR}! \beta_{SR}^{\alpha_{SR}}} \right)^K + \frac{{\Theta_4}^{\alpha_{RD}}}{\alpha_{RD}! \beta_{RD}^{\alpha_{RD}}}. \tag{41}$$

Now, substituting (41) into (36), with some manipulations, we can obtain (40). □

5 Numerical Results

In this section, some numerical results are provided to verify the validity of our analysis in Sections 3 and 4. In all our evaluations, we assume that $P = SNR - 10\lg(\alpha_{XY} \times \beta_{XY})$, $P_J = \frac{P_S}{2}$, $\alpha_{XY} = \alpha$, $\kappa_{XY} = \kappa$, $\sigma_{e_{XY}}^2 = \sigma_e^2$, $\beta_{XY} = \beta = 1$, $\sigma_{XY}^2 = 1$, $\Omega_{XY} = 1$ and $R_S = 0.5$.

Fig. 2 illustrates the OP and IP versus power allocation coefficient μ for different distortion noise parameters ($\kappa = 0, 0.1, 0.15$). The other parameters are set to $\alpha = 2$, $\{\xi_1, \xi_2\} = \{0.02, 0.99\}$, $SNR = 5dB, \sigma_e^2 = 0.05, N = 2$ and $K = 2$. It can be seen that when the power allocation coefficient rises gradually, the outage performance increases, and IP increases with μ increasing. And we can see that the OP is proportional to distortion noise parameter, while IP is inversely proportional to κ. This shows that RHIs has a destructive effect on system performance.

Fig. 3 plots the OP and IP versus the average transmit SNR for different quantization coefficients of the artificial noise $\{\xi_1, \xi_2\} = (\{0.02, 0.99\}; \{0.2, 0.5\})$ under the ideal $\left(\sigma_e^2 = 0, \kappa = 0\right)$ and non-ideal conditions. The exact theoretical curves for the OP and IP are plotted according to (23), (24) and (31), (32). In this simulation, we set $\alpha = 2$, $\mu = 0.8, \sigma_e^2 = 0.1, \kappa = 0.15, N = 2$ and $K = 2$. Clearly, we can see from the simulation results that the outage performance can be worse when ξ_1 increases. Additionally, the OP of imperfect hardware is higher than the ideal case due to the distortion and we can observe that increasing the quantization coefficient ξ_2 of artificial noise will reduce the IP, which means that jammer source is an effective way to increase security. Finally, there exists a trade-off between the reliability and security, which implies that optimal performance exists.

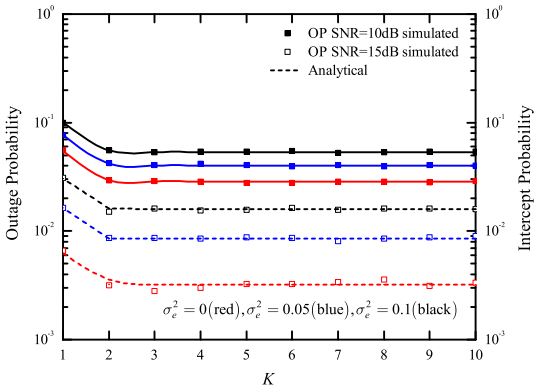

Fig. 4: OP versus K for difference σ_e^2 and SNR ($\alpha = 2, \mu = 0.8, \{\xi_1, \xi_2\} = \{0.06, 0.95\}$ and $\kappa = 0.1$)

Fig. 4 depicts the OP versus the number of the source node antennas K for different CEEs. For this figure, we set $\alpha = 2, \mu = 0.8, \{\xi_1, \xi_2\} = \{0.06, 0.95\}$ and $\kappa = 0.1$. It can be observed that the reliability improves fast as the number of antennas grows when the number of antennas is less than 4. When this number becomes larger than 4, the reliability increases slowly, which means that OTAS is an effective way to improve reliability at a small number of antennas. Additionally, we can also observe that the OP decreases with the increases of SNR, while it increases with the increase of CEEs parameters. Finally, it is shown that the high transmit power yields larger OP gaps for arbitrary CEEs.

In Fig. 5, the IP is plotted versus the number of eavesdropper node antennas for different average transmit SNR values and channel estimation parameters. Here, we set other parameters as shown in Fig. 4. The simulation explained that the eavesdropping ability of the system was weakened with the rise of CEEs and the size of SNR was inversely proportional to the IP. It is also illustrated that the IP in the ideal channel is greater than that in the non-ideal case.

Fig. 6 shows the OP and IP versus transmit SNR in presence of RHIs and CEEs. The parameter values are given as following:

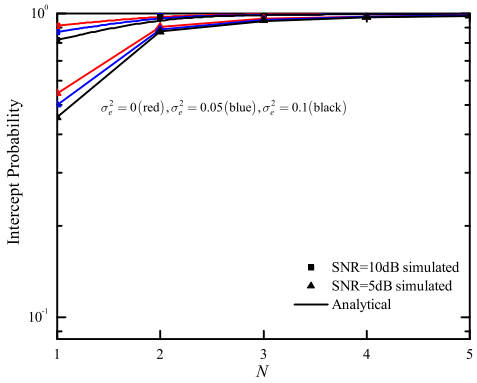

Fig. 5: OP versus N for difference SNR and σ_e^2 ($\alpha = 2$, $\mu = 0.8$, $\{\xi_1, \xi_2\} = \{0.06, 0.95\}$ and $\kappa = 0.1$)

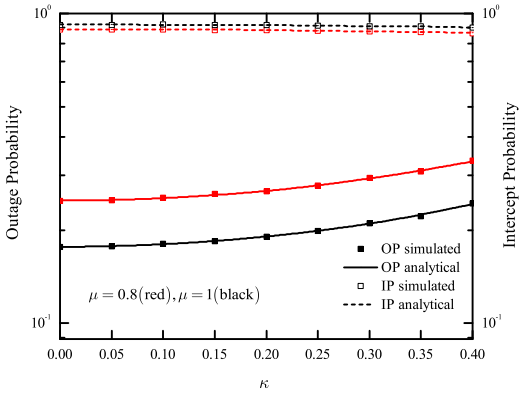

Fig. 7: OP and IP versus distortion noise parameter κ for different μ ($\alpha = 2, SNR = 5dB, \{\xi_1, \xi_2\} = \{0.06, 0.95\}, K = 2, N = 2$ and $\sigma_e^2 = 0.05$)

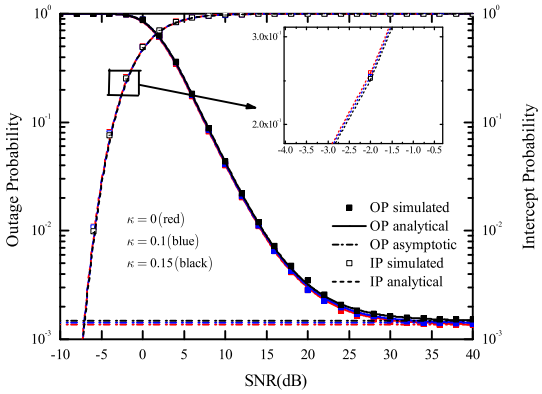

Fig. 6: Simulated OP and IP, analyze them versus SNR for different κ ($\alpha = 2, \mu = 0.8, \{\xi_1, \xi_2\} = \{0.06, 0.95\}, K = 2, N = 2$ and $\sigma_e^2 = 0.05$)

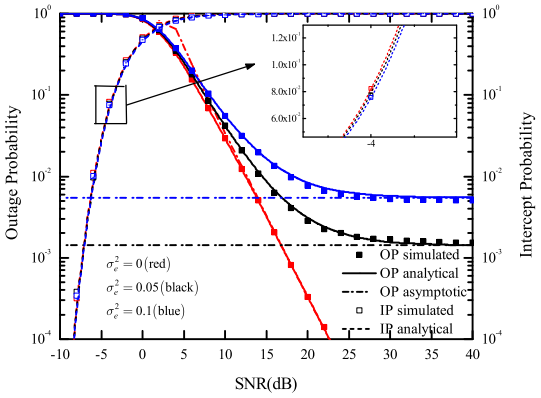

Fig. 8: OP and IP versus SNR for different σ_e^2 ($\alpha = 2, \mu = 0.8, \{\xi_1, \xi_2\} = \{0.06, 0.95\}, K = 2, N = 2$ and $\kappa = 0.1$)

$\alpha = 2, \mu = 0.8, \{\xi_1, \xi_2\} = \{0.06, 0.95\}, K = 2, N = 2$ and $\sigma_e^2 = 0.05$. We clearly see that OP increases as RHIs grows in the multiple antenna conditions, while the IP decreases when the value κ increases, which means RHIs not be good for IP. This figure also shows that there exists error floor for the OP in the non-ideal case. Similarly, there is an optimal transmit SNR value for this case to obtain a trade-off between reliability and security.

Fig. 7 presents the OP and IP versus distortion noise parameter for different power allocation efficients ($\mu = 0.8, 1$). As in [28], we take the range of transceiver distortion noise is $\kappa \in [0, 0.4]$. In this simulation, we set $\alpha = 2, SNR = 5dB, \{\xi_1, \xi_2\} = \{0.06, 0.95\}, K = 2, N = 2$ and $\sigma_e^2 = 0.05$. Fig. 7 shows that the outage performance is broken as κ increases, and the IP becomes worse as κ increases, which means that RHIs can improve the security performance. Similarly, we can also observe that the μ has a negative impact on the OP and a positive effect on the IP.

In Fig. 8, we present the OP and IP versus the average transmit SNR for different CEEs. For comparison, the case of perfect CSI is taken into account ($\sigma_e^2 = 0$). In this simulation, we set $\alpha = 2, \mu = 0.8, \{\xi_1, \xi_2\} = \{0.06, 0.95\}, K = 2, N = 2$ and $\kappa = 0.1$. These results clearly show that the OP increases as σ_e^2 increases, and there exists an error floor under the cases of non-zero σ_e^2. This observation verifies the conclusion of **Remark 1** and **Remark 2**. It can also be observed that the effect of CEEs on the IP is relatively small, which means that the differences of IP among the three values of $\sigma_e^2 = 0$ can be ignored in high and low SNR regions. Finally, we

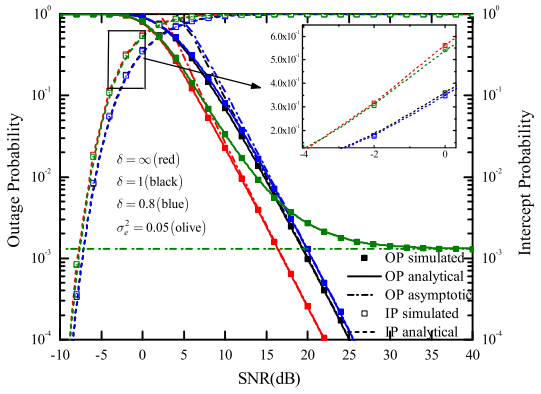

Fig. 9: OP and IP versus SNR for different channel estimation models ($\alpha = 2, \mu = 0.9, \{\xi_1, \xi_2\} = \{0.02, 0.99\}, K = 2, N = 2$ and $\kappa = 0.1$)

can also observe that the OP converges to zero as the average SNR becomes large.

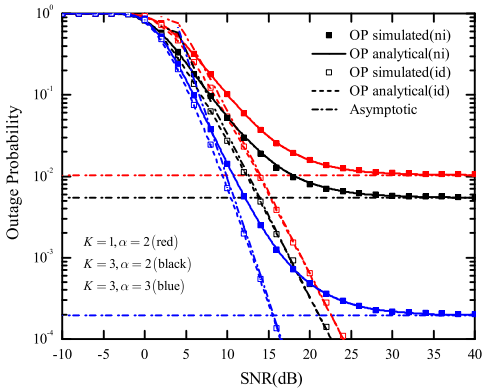

Fig. 10: OP versus SNR for different α and K ($\mu = 0.8, \{\xi_1, \xi_2\} = \{0.02, 0.99\}, \sigma_e^2 = 0.1$ and $\kappa = 0.1$)

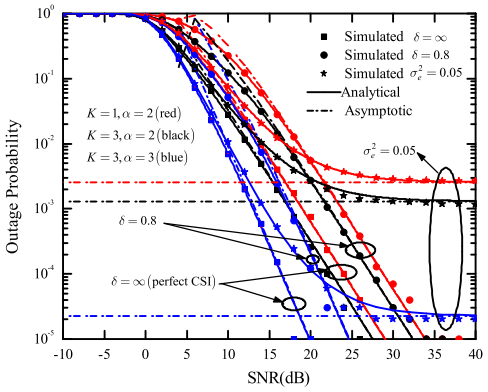

Fig. 11: OP versus SNR for different α, K and σ_e^2 ($\mu = 0.8, \{\xi_1, \xi_2\} = \{0.02, 0.99\}$ and $\kappa = 0.1$)

In Fig. 9, we show the impact of CEEs for the two channel estimation cases. For the first case, we set $\sigma_e^2 = 0.05$; for the second case, we set $\sigma_e^2 = \Omega/(1 + \delta\rho\Omega), \Omega = 1, \delta \in \{0.8, 1\}$. In this simulation, we set $\alpha = 2, \mu = 0.9, \{\xi_1, \xi_2\} = \{0.02, 0.99\}, K = 2, N = 2$ and $\kappa = 0.1$. From these results, we can observe that there exits an error floor for the first case (fixed CEEs), which is determined by the level of estimation errors. For the second case (variable CEEs), there is no error floor in the presence of RHIs and the slopes of asymptotic OP are connected with the K, α_{SR} and α_{RD}, the simulation verified the expressions of (37), (38) and (40). This figure shows that the OP decreases and IP increases with increasing δ. Therefore, we can conclude that CEEs have a detrimental effect on the OP. In addition, for the IP of this figure, we have the following observations: i) the gap of IP between perfect CSI and the second case becomes smaller as the average transmit SNR increases; ii) at low SNR, the IP for the second case less than the first one, vice versa; iii) at high SNRs, the effect of CEEs on the IP is relatively small.

Fig. 10 presents the OP and the asymptotic results versus average transmit SNR for different fading parameters α and antenna numbesr K. Note that in these results, we set $\mu = 0.8$ and $\{\xi_1, \xi_2\} = \{0.02, 0.99\}$. In this simulation, we consider two kinds of conditions: i) ideal ($\kappa = 0$ and $\sigma_e^2 = 0$); ii) non-ideal ($\kappa = 0.1$ and $\sigma_e^2 = 0.1$). We can see that the ideal system outage performance is better than non-ideal. From these results, we can observe that there exit error floors for the non-ideal conditions due to the fixed CEEs, which is irrelevant to the transmit SNR. The asymptotic curves for the OP are plotted according to (33), (34) and (35). For non-ideal conditions: 1) when σ_e^2 is a variable, the slopes of asymptotic OP are not zero, which verifies the analysis of (37) in Section 4; 2) when σ_e^2 is a fixed constant, the slope of the asymptotic OP are zero, which verifies the analysis of (38) in Section 4. For ideal conditions, the slope of the asymptotic OP is a nonzero constant, which verifies the analysis of (40) in Section 4.

Fig. 11 shows the exact and asymptotic OP as a function of the transmit SNR for different values of α, σ_e^2 and K. It can be noticed that: 1) when δ is a fixed value, the slope of the asymptotic OP in the simulation does not change significantly after changing the number of source node antennas; this is because β is 1; 2) when CEEs is a variable, that is, when δ is greater than zero, it can be observed that changing the value of δ does not affect the slope of the curves when other conditions are constant; 3) when other conditions are met, when the α value becomes larger, the diversity orders of the system become larger; 4) when CEEs is constant, the OP has an error floor. These results further verified (37), (38) and (40) in Section 4.

6 Conclusion

In this paper, we have analyzed the effect of RHIs and CEEs on the reliability and security of multi-antenna relay networks in terms of OP and IP. The OTAS strategy and collaborative eavesdropping scheme have been proposed and it was found that the former enhances the reliability and the latter reduces security of the networks. The exact analytical expressions for the OP and IP were derived for the proposed strategy. Numerical results reveal that: 1) the outage performance is weakened as the number of source node antennas increases; 2) the eavesdrop performance is enhanced by the number of source node antenna increases; 3) the OP is inversely proportional to the power allocation coefficient and IP is proportional to the power allocation coefficient; 4) OP increases with the increase of quantization coefficients of the artificial noise, while IP decrease as quantization coefficient increases; 5) we further understand that HIs and CEEs have detrimental impact on system performance; 6) there exists error floor for the OP due to the CEEs.

7 References

1 Zhang D., Zhou Z., Mumtaz S., *et al.*:'One integrated energy efficiency proposal for 5G IoT communications'. IEEE Int. Things J., 2016, **3**, (6), pp. 1346-1354.

2 Zhang W., He W., Wu D., *et al.*:'Joint mode selection, link allocation and power control in underlaying D2D communication'. KSII Trans. Int. Inf. Systems, 2016, **10**, (11), pp. 5209-5228.

3 Lv T., Ma Y., Zeng J., *et al.*:'Millimeter-wave NOMA transmission in cellular M2M communications for Internet of Things'. IEEE Int. Things J., 2018, **5**, (3), pp. 1989-2000.

4 Li X., Li J., Li L., *et al.*:'Performance analysis of cooperative small cell systems under correlated Rician/Gamma fading channels'. IET Signal Process., 2018, **12**, (1), pp. 64-73.

5 Diez F. P., Touceda D. S., Sierra Camara J. M., *et al.*:'Toward self-authenticable wearable devices'. IEEE Wireless Commun., 2015, **22**, (1), pp. 36-43.

6 Chen X., Guo L., Li X., *et al.*:'Secrecy rate optimization for cooperative cognitive radio networks aided by a wireless energy harvesting jammer'. IEEE Access, 2018, pp. 34127-34134.

7 Wyner A. D.:'The wire-tap channel'. Bell Syst. Tech. J., 1975, **54**, (8), pp. 1355-1387.

8 Ammari M., Fortier P.:'Physical layer security of multiple-input-multiple-output systems with transmit beamforming in Rayleigh fading'. IET Commun., 2015, **9**, (8), pp. 1096-1103.

9 Ahmed M., Bai L.:'Secrecy capacity of artificial noise aided secure communication in MIMO Rician channels'. IEEE Access, 2018, **6**, pp. 7921-7929.

10 Lei H., Gao C.,Guo Y., *et al.*:'On physical layer security over generalized Gamma fading channels'. IEEE Commun. Lett., 2015, **19**, (7), pp. 1257-1260.

11 Lei H., Ansari I. S., Pan G., *et al.*:'Secrecy capacity analysis over $\alpha - \mu$ fading channels'. IEEE Commun. Lett., 2017, **21**, (6), pp. 1445-1448.

12 Sun J., Li X., Huang M., *et al.*:'Performance analysis of physical layer security over $\kappa - \mu$ shadowed fading channels'. IET Commun., 2018, **12**, (8), pp. 970-975.

13 Liu K. R.:'Cooperative communications and networking'. Cambridge Univ. Press, 2009.

14 Deng C., Zhao X., Zhang D., *et al.*:'Performance analysis of NOMA-based relaying networks with transceiver hardware impairments'. KSII Trans. Int. Inf. Systems, 2018.

15 Li X., Li J., Li L., *et al.*:'Performance analysis of impaired SWIPT NOMA relaying networks over imperfect Weibull channels'. IEEE Syst. J., 2019, **99**, (99), pp. 1-4.

16 Wu L., Yang L., Chen J., *et al.*:'Physical layer security for cooperative relaying over Generalized-K fading channels'. IEEE Wireless Commun. Lett., 2018, pp. 1-4.

17 Zou Y., Wang X., Shen W.:'Optimal relay selection for physical layer security in cooperative wireless networks'. IEEE J. Sel. Areas Commun., 2013, **31**, (10), pp.

2099-2111.
18 Son P. N., Kong H. Y.:'Cooperative communication with energy harvesting relays under physical layer security'. IET Commun., 2015, **9**, (17), pp. 2131-2139.
19 Asaad S., Bereyhi A., Rabiei A., *et al.*:'Optimal transmit antenna selection for massive MIMO wiretap channels '. IEEE J. Sel. Areas Commun., 2018, **36**, (4), pp. 817-828.
20 Peters S., Heath R..:'Nonregenerative MIMO relaying with optimal transmit antenna selection'. IEEE Signal Process. Lett., 2008, **15**, pp. 421-424.
21 Lei H., Zhang J., Park K., *et al.*:'On secure NOMA systems with transmit antenna selection schemes'. IEEE Access, 2017, **5**, pp. 17450-17464.
22 Liu Y., Qin Z., Elkashlan M., *et al.*:'Enhancing the physical layer security of non-orthogonal multiple access in large-scale networks'. IEEE Trans. Wireless. Commun., 2017, **16**, (3), pp. 1656-1672.
23 Lei H., Zhang H., Ansari I., *et al.*:'On secrecy outage of relay selection in underlay cognitive radio networks over Nakagami-m fading channels'. IEEE Trans. Cogn. Commun. Netw., 2017, **3**, (4), pp. 614-627.
24 Zhang H., Lei H., Ansari I., *et al.*:'Security performance analysis of DF cooperative relay networks over Nakagami-m fading channels'. KSII Trans. Int. Inf. Systems, 2017, pp. 2416-2432.
25 Tang X., Yang W., Y. Cai., *et al.*:'Security of full-duplex jamming SWIPT system with multiple non-colluding eavesdroppers'. 7th IEEE Int. Conf. Elec. Inf. Emerg. Commun. (ICEIEC), 2017, pp: 66-69.
26 Yeoh P. L. , Yang N. , Kim K. J.:'Secrecy outage probability of selective relaying wiretap channels with collaborative eavesdropping'. IEEE Global Commun. Conf. (GLOBECOM), 2015, pp: 1-6.
27 Schenk T.:'RF imperfections in high-rate wireless systems: Impact and digital compensation'. Eindhoven, Netherland: Springer, 2008.
28 Li X., Huang M.,Tian X., *et al.*:'Impact of hardware impairments on large-scale MIMO systems over composite RG fading channels'. AEU-Int. J. Electron. Commun., 2018, **88**, pp. 134-140.
29 Bjornson E., Hoydis J., Kountouris M., *et al.*:'Massive MIMO systems with non-ideal hardware: energy efficiency, estimation, and capacity limits'. IEEE Trans. Inf. Theory, 2014, **60**, (11), pp. 7112-7139.
30 Li X., Li J., Jin J., *et al.*:'Performance analysis of relaying systems over Nakagami-m fading with transceiver hardware impairments'. Xian Dianzi Keji Daxue journal of Xidian Univ., 2017, **25**, (3), pp. 135-140.
31 Studer C.,Wenk M., Burg A.:'MIMO transmission with residual transmit-RF impairments'. Proc. ITG/IEEE Workshop Smart Antennas, 2010, pp. 189-196.
32 Li X., Matthaiou M., Liu Y., *et al.*:'Multi-pair two-way massive MIMO relaying with hardware impairments over Rician fading channels'. IEEE Global Commun. Conf. (GLOBECOM), 2018.
33 Li X., Li J., Mathiopoulos P. T., *et al.*:'Joint impact of hardware imperfect CSI on cooperative SWIPT NOMA multi-relaying system'. IEEE ICCC/CIC, Beijing, 2018.
34 Li X., Li J., Liu Y., *et al.*:'Outage performance of cooperative NOMA networks with hardware impairments'. IEEE Global Commun. Conf. (GLOBECOM), 2018.
35 Yang T., Zhang R., Cheng X., *et al.*:'Secure massive MIMO under imperfect CSI: performance analysis and channel prediction'. IEEE Trans. Inf. Forensics Security, 2019, **14**, (6), pp. 1610-1623.
36 Yang T., Zhang R., Cheng X., *et al.*:'Performance analysis of secure communication in massive MIMO with imperfect channel state information'. IEEE International Conference on Communications (ICC), 2018, pp. 1-6.
37 Ding X., Song T., Zou Y., *et al.*:'Security-reliability tradeoff analysis of artificial noise aided two-way opportunistic relay selection'. IEEE Trans. Veh. Technol., 2017, **66**, (5), pp. 3930-3941.
38 Gabry F., Thobaben R., Skoglund M.:'Outage performances for amplify-and-forward, decode-and-forward and cooperative jamming strategies for the wiretap channel'. IEEE Wireless Commun. Netw. Conf., Cancun, Quintana Roo, 2011, pp. 1328-1333.
39 Peng L., Zang G., Zhou Q., *et al.*:'Security performance analysis for cooperative communication system under Nakagami-m fading channel'. IEEE 17th Int. Conf. Commun. Technol., 2017, pp. 187-192.
40 Bjornson E., Matthaiou M., Debbah M.:'A new look at dual-hop relaying : performance limits with hardware impairments'. IEEE Trans. Commun., 2013, **61**, (11), pp. 4512-4525.
41 Goldsmith A.:'Wireless communications[M]'. Cambridge university press, 2005.
42 Liu Y., Ding Z., Elkashlan M., *et al.*:'Cooperative nonorthogonal multiple access with simultaneous wireless information and power transfer'. IEEE J. Sel. Areas Commun., 2016, **34**, (4), pp. 938-953.
43 Chen Z., Chi Z., Li Y., *et al.*:'Error performance of maximal-ratio combining with transmit antenna selection in flat Nakagami-m fading channels'. IEEE Trans. Wireless Commun., 2009, **8**, (1), pp. 424-431.

8 Acknowledgments

This work was supported in part by the National Natural Science Foundation of China under Grant 61601414, in party by the Henan Scientific and Technological Research Project (182102210307), in party by Doctoral Scientific Funds of Henan polytechnic University (B2016-34), in party by Fundamental Research Funds for the Universities of Henan Province (NSFRF180309) and in party by the Outstanding Youth Science Foundation of Henan Polytechnic University (J2019-4).

9 Appendix A

The proof of theorem 1 is given in this section.

Proof: According to the relevant mathematical knowledge, we can turn (22) into the following formula:

$$\begin{aligned} P_{\text{out}} &= 1-\Pr\left\{\min\left(C_{SR},C_{RD}\right)>R_S\right\} \\ &= \underbrace{\Pr\{C_{SR}<R_S\}}_{I_1}+\underbrace{\Pr\{C_{RD}<R_S\}}_{I_2}-\underbrace{\Pr\{C_{SR}<R_S\}}_{I_1}\underbrace{\Pr\left\{C_{RD}<R_S\right\}}_{I_2}. \end{aligned} \tag{A.1}$$

Then, set $\varepsilon = 2^{2R_S}-1$ in the following calculations of I_1 and I_2.

Firstly, substitute (20) to (A.1), we can derive the formula follows:

$$\begin{aligned} I_1 &= \Pr\left\{\frac{1}{2}\log_2\left(1+\frac{\left|\hat{h}_{SR}\right|^2\rho_{SR}}{\rho_{SR}\left(\sigma_{e_{SR}}^2+\left|\hat{h}_{SR}\right|^2\kappa_{SR}^2+\sigma_{e_{SR}}^2\kappa_{SR}^2\right)+1}\right)<R_S\right\} \\ &= \Pr\left\{\left|\hat{h}_{SR}\right|^2<\underbrace{\frac{\varepsilon\rho_{SR}\sigma_{e_{SR}}^2\left(1+\kappa_{SR}^2\right)+\varepsilon}{\rho_{SR}\left(1-\varepsilon\kappa_{SR}^2\right)}}_{\Theta_1}\right\}. \end{aligned} \tag{A.2}$$

In what follows, I_1 will be addressed. According to (18), I_1 can be calculated as:

$$\begin{aligned} I_1 &= \Pr\left\{\left|\hat{h}_{SR}\right|^2<\Theta_1\right\} = F_{\left|\hat{h}_{SR}\right|^2}\left(\Theta_1\right) \\ &= \left[1-\sum_{j=0}^{\alpha_{SR}-1}\frac{e^{-\frac{\Theta_1}{\beta_{SR}}}}{j!}\left(\frac{\Theta_1}{\beta_{SR}}\right)^j\right]^K. \end{aligned} \tag{A.3}$$

Secondly, substituting (21) to (A.1), we can get the following formula:

$$\begin{aligned} I_2 &= \Pr\left\{\frac{\rho_{RD}\left|\hat{h}_{RD}\right|^2}{\sigma_{e_{RD}}^2\rho_{RD}+\left(\xi_1 P_J\middle/\sigma_{RD}^2+\kappa_{RD}^2\rho_{RD}\right)\left(\left|\hat{h}_{RD}\right|^2+\sigma_{e_{RD}}^2\right)+1}<\varepsilon\right\} \\ &= \Pr\left\{\left|\hat{h}_{RD}\right|^2<\underbrace{\frac{\varepsilon\left[\sigma_{e_{RD}}^2\left(\rho_{RD}+\xi_1 P_J\middle/\sigma_{RD}^2+\kappa_{RD}^2\rho_{RD}\right)+1\right]}{\rho_{RD}-\varepsilon\left(\xi_1 P_J\middle/\sigma_{RD}^2+\kappa_{RD}^2\rho_{RD}\right)}}_{\Theta_2}\right\}, \end{aligned} \tag{A.4}$$

in this case, I_2 will be computed. Similarly, according to (14), I_2 is calculated as:

$$\begin{aligned} I_2 &= \Pr\left\{\left|\hat{h}_{RD}\right|^2<\Theta_2\right\} = F_{\left|\hat{h}_{RD}\right|^2}\left(\Theta_2\right) \\ &= 1-\sum_{l=0}^{\alpha_{RD}-1}\frac{e^{-\frac{\Theta_2}{\beta_{RD}}}}{l!}\left(\frac{\Theta_2}{\beta_{RD}}\right)^l. \end{aligned} \tag{A.5}$$

Substituting (A.3) and (A.5) into (A.1), we can obtain the (23).

For ideal condition, we can get the expression of (24) by set $\kappa_{SR}=\kappa_{RD}=0$ and $\sigma_{e_{SR}}^2=\sigma_{e_{RD}}^2=0$. □

10 Appendix B

The proof of theorem 2 is given in this section.

Proof: Collaborative eavesdropper scheme

1) Non-independent identical distribution

In the case of low SNR, (27) can be approximated as

$$P_{\text{int,asy}}^{\text{n.i.i.d}} = \Pr\left\{\sum_{n=1}^{N}\left|\hat{h}_{RE_n}\right|^2 > \frac{\varepsilon}{\rho_{RE_n}}\right\}, \tag{B.1}$$

in addition, the PDF of $\sum_{n=1}^{N}\left|\hat{h}_{RE_n}\right|^2$ can be easily obtained as [43]

$$f_{\sum_{n=1}^{N}\left|\hat{h}_{RE_n}\right|^2}(x) = \frac{x^{N\alpha_{RE_n}-1}e^{-\frac{x}{\beta_{RE_n}}}}{\Gamma\left(N\alpha_{RE_n}\right)\beta_{RE_n}^{N\alpha_{RE_n}}}. \tag{B.2}$$

Substituting (B.2) into (B.1), the (28) can be obtained.

2) Independent identical distribution

Similar to Appendix A, substituting (12) into (15) and put (30) into (25), we can get the formula as follows:

$$\begin{aligned}P_{\text{int,i.i.d}}^{\text{ni}} &= \Pr\left\{\frac{N\rho_{RE_n}\left|\hat{h}_{RE_n}\right|^2}{\sigma_{e_{RE_n}}^2\rho_{RE_n}+\left(\frac{\xi_2 P_J}{\sigma_{RE_n}^2}+\kappa_{RE_n}^2\rho_{RE_n}\right)\left(\left|\hat{h}_{RE_n}\right|^2+\sigma_{e_{RE_n}}^2\right)+1} > \varepsilon\right\}\\ &= 1-\Pr\left\{\left|\hat{h}_{RE_n}\right|^2 < \underbrace{\frac{\varphi\left[\sigma_{e_{RE_n}}^2\left(\rho_{RE_n}+\frac{\xi_2 P_J}{\sigma_{RE_n}^2}+\kappa_{RE_n}^2\rho_{RE_n}\right)+1\right]}{\rho_{RE_n}-\varphi\left(\frac{\xi_2 P_J}{\sigma_{RE_n}^2}+\kappa_{RE_n}^2\rho_{RE_n}\right)}}_{\Theta_5}\right\}\\ &= 1-F_{\left|\hat{h}_{RE_n}\right|^2}(\Theta_5),\end{aligned} \tag{B.3}$$

Substituting (14) into (B.3), we can obtain the (31).

For ideal condition, we can get the expression of (32) by set $\kappa_{RE_n}=0$ and $\sigma_{e_{RE_n}}^2=0$. □

11 Appendix C

The proof of Corollary 1 is given in this section.

Proof: A. Non-ideal condition

1) When $\sigma_{e_{XY}}^2 = \frac{\Omega_{XY}}{1+\delta\rho_{XY}\Omega_{XY}}$

In a similar methodology to [4], (13) can be extended to Taylor's form. When $\rho_{XY}\to\infty$, Only the first summation of an infinite series is the dominant term. Thus, (13) and (14) can be further simplified respectively as:

$$f_{\left|\hat{h}_{XY}\right|^2}(x) = \frac{x^{\alpha_{XY}-1}}{\Gamma\left(\alpha_{XY}\right)\beta_{XY}^{\alpha_{XY}}} + o(x), x>0, \tag{C.1}$$

$$F_{\left|\hat{h}_{XY}\right|^2}(x) \approx \frac{x^{\alpha_{XY}}}{\alpha_{XY}!\beta_{XY}^{\alpha_{XY}}} + o(x), x>0. \tag{C.2}$$

According to (C.2), we can get the CDF of maximum channel gain after being selected under high SNR as following:

$$F_{\left|\hat{h}_{SR}\right|^2}^{\infty,\text{ni}}(x) \approx \left(\frac{x^{\alpha_{SR}}}{\alpha_{SR}!\beta_{SR}^{\alpha_{SR}}}\right)^K. \tag{C.3}$$

By the definition of OP in Section 3, we can get the following formulas:

$$I_3 = F_{\left|\hat{h}_{SR}\right|}^{\infty,\text{ni}}(\Theta_1) = \left(\frac{{\Theta_1}^{\alpha_{SR}}}{\alpha_{SR}!\beta_{SR}^{\alpha_{SR}}}\right)^K, \tag{C.4}$$

$$I_4 = F_{\left|\hat{h}_{RD}\right|}^{\infty,\text{ni}}(\Theta_2) = \frac{{\Theta_2}^{\alpha_{RD}}}{\alpha_{RD}!\beta_{RD}^{\alpha_{RD}}}. \tag{C.5}$$

Thus, we can derive the asymptotic expression of OP under high SNRs as:

$$\begin{aligned}P_{\text{out}}^{\infty,\text{ni1}} &= I_3 + I_4 - I_3 I_4\\ &= \left(\frac{{\Theta_1}^{\alpha_{SR}}}{\alpha_{SR}!\beta_{SR}^{\alpha_{SR}}}\right)^K + \frac{{\Theta_2}^{\alpha_{RD}}}{\alpha_{RD}!\beta_{RD}^{\alpha_{RD}}} - \left(\frac{{\Theta_1}^{\alpha_{SR}}}{\alpha_{SR}!\beta_{SR}^{\alpha_{SR}}}\right)^K\left(\frac{{\Theta_2}^{\alpha_{RD}}}{\alpha_{RD}!\beta_{RD}^{\alpha_{RD}}}\right).\end{aligned} \tag{C.6}$$

2) When $\sigma_{e_{XY}}^2 = a$ (a is a constant):

According to (20), (21) and $P_J = \frac{P_R}{2}$, we can derived the channel capacity expressions of first slot and from R to D under high SNRs ($\rho_{XY}\to\infty$) as:

$$C_{SR}^{\infty,\text{ni}} = \frac{1}{2}\log_2\left(1+\frac{\left|\hat{h}_{SR}\right|^2}{\sigma_{e_{SR}}^2+\kappa_{SR}^2\left(\left|\hat{h}_{SR}\right|^2+\sigma_{e_{SR}}^2\right)}\right), \tag{C.7}$$

$$C_{RD}^{\infty,\text{ni}} = \frac{1}{2}\log_2\left(1+\frac{\left|\hat{h}_{RD}\right|^2}{\sigma_{e_{RD}}^2+\left(\xi_1/2+\kappa_{RD}^2\right)\left(\left|\hat{h}_{RD}\right|^2+\sigma_{e_{RD}}^2\right)}\right). \tag{C.8}$$

According to the definition of OP in Section 3, we can get the following:

$$P_{\text{out}}^{\infty,\text{ni2}} = \Pr\left\{\min\left(C_{SR}^{\infty,\text{ni}}, C_{RD}^{\infty,\text{ni}}\right) < R_S\right\}, \tag{C.9}$$

and then, we can derive the following formula:

$$\begin{aligned}P_{\text{out}}^{\infty,\text{ni2}} &= \underbrace{\Pr\left\{C_{SR}^{\infty,\text{ni}} < R_S\right\}}_{I_5} + \underbrace{\Pr\left\{C_{RD}^{\infty,\text{ni}} < R_S\right\}}_{I_6}\\ &\quad - \underbrace{\Pr\left\{C_{SR}^{\infty,\text{ni}} < R_S\right\}}_{I_5}\underbrace{\Pr\left\{C_{RD}^{\infty,\text{ni}} < R_S\right\}}_{I_6}.\end{aligned} \tag{C.10}$$

.

Similarly to the Appendix A, we can derive the expressions of I_3 and I_4 as:

$$\begin{aligned}I_5 &= \Pr\left\{\frac{1}{2}\log_2\left(1+\frac{\left|\hat{h}_{SR}\right|^2}{\sigma_{e_{SR}}^2+\kappa_{SR}^2\left(\left|\hat{h}_{SR}\right|^2+\sigma_{e_{SR}}^2\right)}\right) < R_S\right\}\\ &= \Pr\left\{\left|\hat{h}_{SR}\right|^2 < \underbrace{\frac{\varepsilon\sigma_{e_{SR}}^2\left(1+\kappa_{SR}^2\right)}{1-\varepsilon\kappa_{SR}^2}}_{\Theta_7}\right\},\end{aligned} \tag{C.11}$$

then, substituting (19), we can derive the following expression of I_3 as:

$$\begin{aligned}I_5 &= \Pr\left\{\left|\hat{h}_{SR}\right|^2 < \Theta_7\right\} = F_{\left|\hat{h}_{SR}\right|^2}(\Theta_7)\\ &= \left[1-\sum_{j=0}^{\alpha_{SR}-1}\frac{e^{-\frac{\Theta_7}{\beta_{SR}}}}{j!}\left(\frac{\Theta_7}{\beta_{SR}}\right)^j\right]^K,\end{aligned} \tag{C.12}$$

Similarly, we can deduce that I_6 is equal to the following formula:

$$I_6 = \Pr\left\{\frac{\left|\hat{h}_{RD}\right|^2}{\sigma_{e_{RD}}^2 + \left(\xi_1/2+\kappa_{RD}^2\right)\left(\left|\hat{h}_{RD}\right|^2+\sigma_{e_{RD}}^2\right)} < \varepsilon\right\}$$
$$= \Pr\left\{\left|\hat{h}_{RD}\right|^2 < \underbrace{\frac{\varepsilon\sigma_{e_{RD}}^2\left(1+\xi_1/2+\kappa_{RD}^2\right)}{1-\varepsilon\xi_1/2-\varepsilon\kappa_{RD}^2}}_{\Theta_8}\right\}, \tag{C.13}$$

substituting (14) into (C.13), we can derive the expression of I_4 as:

$$I_6 = \Pr\left\{\left|\hat{h}_{RD}\right|^2 < \Theta_8\right\} = F_{\left|\hat{h}_{RD}\right|^2}(\Theta_8)$$
$$= 1 - \sum_{l=0}^{\alpha_{RD}-1} \frac{e^{-\frac{\Theta_8}{\beta_{RD}}}}{l!}\left(\frac{\Theta_8}{\beta_{RD}}\right)^l. \tag{C.14}$$

Substituting (C.12) and (C.14) into (C.9), we can get the expression of (34).

B. Ideal condition

Similar to what we did in case $\sigma_{e_{XY}}^2 = \frac{\Omega_{XY}}{1+\delta\rho_{XY}\Omega_{XY}}$, we can derive the asymptotic expression of OP under high SNRs as:

$$P_{\text{out}}^{\infty,\text{id}} = I_7 + I_8 - I_7 I_8 \tag{C.15}$$
$$= \left(\frac{\Theta_3{}^{\alpha_{SR}}}{\alpha_{SR}!\beta_{SR}^{\alpha_{SR}}}\right)^K + \frac{\Theta_4{}^{\alpha_{RD}}}{\alpha_{RD}!\beta_{RD}^{\alpha_{RD}}} - \left(\frac{\Theta_3{}^{\alpha_{SR}}}{\alpha_{SR}!\beta_{SR}^{\alpha_{SR}}}\right)^K\left(\frac{\Theta_4{}^{\alpha_{RD}}}{\alpha_{RD}!\beta_{RD}^{\alpha_{RD}}}\right).$$

□